Article

Establishment of a Dual-Signal Enhanced Fluorescent Aptasensor for Highly Sensitive Detection of Ochratoxin A

Xueying Li, Te Li, Jiahuai Zhang, Qing Zhang, Kai Deng, Runran Ma, Jiabo Wang, and Weijun Kong*
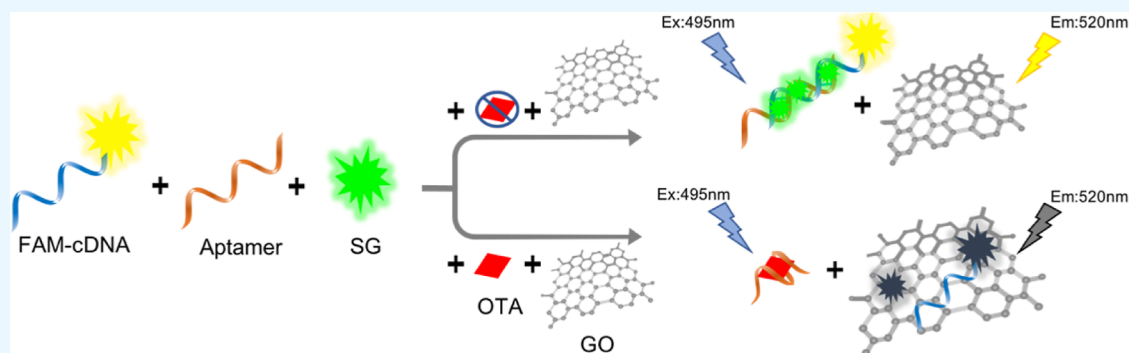
Read Online

ACCESS | Metrics & More | Article Recommendations

ABSTRACT: A robust and versatile dual-signal enhanced fluorescent aptasensor was developed for ochratoxin A (OTA) detection based on fluorescence resonance energy transfer between 5-carboxyfluorescein (FAM) and Super Green I (SG) fluorophores as the donor and graphene oxide (GO) nanosheet as the acceptor. Abundant SG probes were adsorbed into the FAM-complementary DNA (cDNA)-aptamer double-stranded structure to achieve remarkably enhanced fluorescence responses. Without OTA, the FAM-cDNA-SG conjugates coexisted with GO nanosheets, exhibiting strong fluorescence signals. In the presence of OTA, it was captured by the aptamers to release cDNA-FAM and SG probes, which were adsorbed by GO, leading to OTA-dependent fluorescence quenching. The changed fluorescence intensity was measured for accurate quantitation of OTA. Under optimum conditions, the dual-signal enhanced fluorescent aptasensor realized fascinating sensitivity with a limit of detection of 0.005 ng/mL and a wide concentration range of 0.02−20 ng/mL, as well as high selectivity for OTA over other interfering substances, excellent accuracy with average recoveries of 91.37−116.83% in the fortified malt matrices, and superior reliability and practicability in actual samples. This FAM-cDNA-aptamer-SG/GO nanosheet-based aptasensing platform could be extended to monitor other contaminants or trace molecules in food, environmental, and diagnostic fields by altering the corresponding aptamers.

1. INTRODUCTION

Ochratoxin A (OTA) is the most toxic member of ochratoxins naturally generated by *Aspergillus* and *Penicillium* species.[1] It is prevalently found in food, feed, and other commodities.[2,3] Due to its neurotoxic, nephrotoxic, teratogenic, and carcinogenic toxicities and potential risks to human and animal health, OTA has been listed as a 2B carcinogen by the International Agency for Research on Cancer.[4] Consumption of OTA-contaminated products will inevitably lead to tissue bioaccumulation and serious harm.[5] For safeguarding human health from OTA, the regulatory guidelines and maximum residue levels (MRLs) regarding it in certain commodities have been stipulated in the world.[6] To meet these strict requirements and lower the risk of OTA consumption, effective and reliable approaches and analytical methods are urgently required for the sensitive detection of OTA at trace levels (ppt−ppb) in diverse matrices.

Although diverse analytical techniques with fascinating specificity, sensitivity, and repeatability have been constructed for OTA detection,[7−9] they generally require expensive instruments, trained operators, tedious sample pretreatment, high cost, and problematic cross-reactivity. As an appealing alternative strategy, an aptamer-based fluorescent sensor, abbreviated as fluorescent aptasensor, with aptamer as the recognition element to capture the target and fluorescence technique to measure the resulted signal for quantitation has attracted extensive attention in different fields,[10−12] displaying well-received merits of incredible simplicity, easy operation,
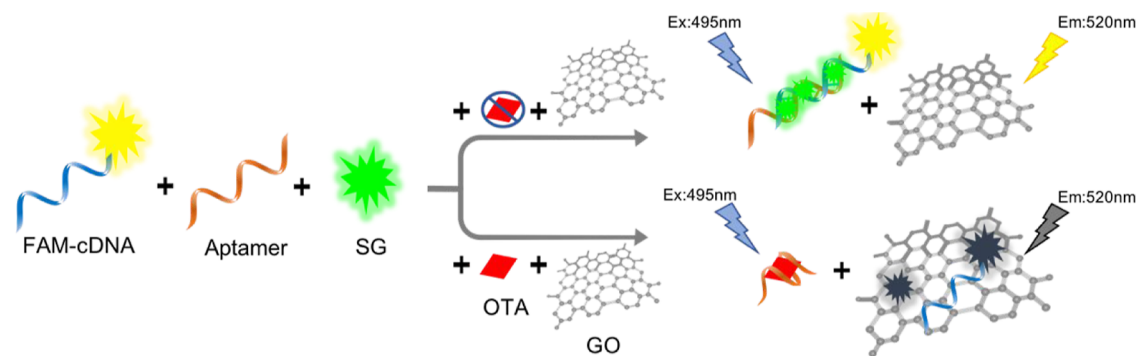
Scheme 1. Dual Fluorescence Auxiliary Signal Amplification Strategy-Based Aptasensor for OTA Detection

rapid responses, low-cost, high sensitivity, and efficient miniaturization for on-site monitoring. In this sensing system, aptamer (Apt) is extremely vital for specifically capturing target molecules to form a three-dimensional folding structure to eliminate the interferences of other molecules, exhibiting high resistance to denaturation and high binding affinity with different targets.[1,13]

Among various nanomaterials in fabricating the fluorescent aptasensing platform, graphene oxide (GO) with a large two-dimensional (2-D) conjugate structure, easily modified surface, good biocompatibility, and excellent dispersibility in water is commonly used as an excellent energy acceptor for effectively quenching the fluorescence of various fluorophores including carboxyfluorescein (FAM) through fluorescence resonance energy transfer (FRET).[10,14] More excitingly, single-stranded DNA (ssDNA) like aptamer can be adsorbed onto the surface of GO through hydrophobic and $\pi-\pi$ stacking interactions.[10,15] Then, FAM-labeled aptamer can be assembled on GO to completely quench the fluorescence of FAM, and GO is regarded as an excellent signal enhancer to improve the performance of the developing fluorescent sensing platforms.[10,14,16,17] In addition, it is worth to note that SYBR Green I (SG), a classic DNA-staining dye with low toxicity and high safety, does not interact with ssDNA; however, its fluorescence response is amplified about 1000 times when it binds to double-stranded DNA.[18,19] Thus, the combination of FAM and SG can remarkably enhance the fluorescence signal under the same exciting wavelength due to the synergistic effect resulting from their very close even same excitation and emission wavelengths, further improving detection sensitivity.

In this study, a FAM and SG dual-signal enhanced fluorescent aptasensor was developed for trace detection of OTA based on FRET between FAM as the donor and GO nanosheet as the acceptor (Scheme 1). First of all, the FAM-labeled complementary DNA (FAM-cDNA) probe and OTA aptamer were combined to form the double-stranded aptamer-cDNA structure. Then, SG was added and inserted into the double-stranded structure, and the FAM-cDNA-aptamer-SG composite system was not adsorbed onto the GO nanosheet without fluorescence quenching. Under the UV excitation at 495 nm, both SG and FAM emitted strong fluorescence responses at an emission wavelength of 520 nm, leading to a significantly amplified fluorescence signal owing to the synergistic effect. However, with the addition of target OTA, it competitively binds with the aptamer, causing the disassembly of the double-stranded structure and the release of FAM-cDNA and SG. Thereafter, FAM-cDNA was adsorbed onto the GO nanosheet via $\pi-\pi$ stacking interaction.

Consequently, the fluorescence of FAM-cDNA and SG probes was efficiently quenched by GO. By recording the changed fluorescence intensity induced by the added OTA, accurate quantitation of OTA was achieved. Practical application of the developed FAM-cDNA-aptamer-SG/GO nanosheet-based ultrasensitive fluorescent aptasensor in actual edible and medicinal malt[2] samples regarding OTA determination confirmed its great potential for trace contaminants in more complex matrices by altering the corresponding aptamers.

2. MATERIALS AND METHODS

2.1. Materials and Reagents. The OTA aptamer and FAM-labeled cDNA were synthesized and purified by HPLC at the Shanghai Sangon Biotechnology Company, Ltd. (Shanghai, China). The sequence of the OTA aptamer was 5′-GAT CGG GTG TGG GTG GCG TAA AGG GAG CAT CGG ACA-3′, and the sequence of FAM-labeled cDNA was 5′-FAM-TGT CCG ATG CTC CCT TTA CGC CAC CCA CAC CCG ATC-3′. 10,000× SUPER Green I (SG) nucleic acid gel stain was obtained from Mei5 Biotechnology Co., Ltd. (Beijing, China). GO nanosheet solution was purchased from Nanjing XF Nano Material Tech Co., Ltd. (Nanjing, China). OTA, deoxynivalenol (DON), zearalenone (ZEN), aflatoxin B_1 (AFB$_1$), and T-2 toxin (T-2) were purchased from Qingdao Pribolab Biological Engineering Co. Ltd. (Qingdao, China). One M Tris-HCl (1 M, pH 7.4−7.6) was obtained from Shanghai Sangon Biotechnology Co., Ltd. All other chemical reagents were of analytical grade. The buffer solution of the reaction system (10 mM Tris−HCl, 120 mM NaCl, 20 mM CaCl$_2$, 5 mM KCl, at pH 8.5) was freshly prepared. OTA-free malt samples without visible mold were collected from a local medicinal material market in Beijing, China. The moldy malt samples were cultivated in a laboratory incubator box.

2.2. Instrumentation. All fluorescence spectra were measured on an FL970 fluorophotometer (Techcomp, China) equipped with FL Analyze 4.0 software. The excitation and emission slit widths were set to 5 nm. Fluorescence intensities were recorded at 520 nm with an excitation wavelength of 495 nm. UV−vis spectra were measured on a UV−vis spectrophotometer (UV-2550, Shanghai Linli Instrument CO., Ltd., China).

2.3. Preparation of Detection Solutions. The buffer solution containing 10 mM Tris-HCl, 120 mM NaCl, 20 mM CaCl$_2$, and 5 mM KCl was first prepared at pH 8.5. Then, solution a of FAM-cDNA probe (50 μL, 1 μM) and solution b containing FAM-cDNA (50 μL, 1 μM) and SG (2 μL, 100×) probes were prepared in buffer, respectively. The OTA aptamer (50 μL, 1 μM) and FAM-cDNA (50 μL, 1 μM)

probes at a concentration ratio of 1:1 were mixed and incubated in the buffer solution at 37 °C for 1 h to obtain solution *c*. Finally, the OTA aptamer (50 μL, 1 μM), FAM-cDNA (50 μL, 1 μM), and SG (2 μL, 100×) probes were coincubated in the buffer solution at 37 °C for 1 h to prepare solution *d*. All of the solutions were adopted to the final volume of 300 μL.

2.4. Establishment of the Dual-Signal Fluorescent Aptasensor for OTA Detection. The dual-signal enhanced fluorescent aptasensor was established based on the following procedure for OTA detection. The OTA aptamer and FAM-cDNA solutions at the same concentration (50 μL, 1 μM) were mixed with the SG (2 μL, 100×) probe solution in a brown centrifuge tube and incubated at 37 °C with slight shaking for 50 min. Then, the fluorescence intensity (F_1) of this solution in the emission wavelength range of 495−580 nm was determined at an excitation wavelength of 495 nm. After the addition of 30 μL of different concentrations of OTA and incubation under slight shaking for 1 h at 37 °C, the GO nanosheet (10 μL, 1 mg/mL) solution was also added into the centrifuge tube and incubated at 37 °C for 40 min. The fluorescence intensity (F_2) of the final solution system was also determined to establish the dual-signal enhanced fluorescent aptasensor for OTA detection based on the competitive principle according to the obtained standard curve between the difference value (ΔF) of F_1 and F_2 and added concentration of OTA.

2.5. Specificity Assessment. To assess the selectivity and specificity of the dual-signal enhanced fluorescent aptasensor for OTA, some commonly found mycotoxins including DON, ZEN, AFB$_1$, and T-2 toxin were regarded as interferents. Thirty μL of AFB$_1$, ZEN, DON, and T-2 toxin (all at a concentration of 100 ng/mL), as well as OTA (20 ng/mL), was added into the FAM-cDNA-aptamer-SG/GO nanosheet system, respectively, to measure the fluorescence spectrum and record fluorescence intensity to calculate the fluorescence difference value (ΔF).

2.6. Real Sample Analysis. To evaluate the feasibility of the FAM-cDNA-aptamer-SG/GO nanosheet-based fluorescent aptasensor in real analysis, 10 batches of malt samples were randomly selected. Among them, 5 batches of samples were incubated in an environment with high humidity and constant temperature for 7 days until obvious mold flora was observed on the sample surface. Then, all 10 batches of samples were collected and ground into powder and passed through a 1 mm aperture of sieve. One g of malt powder was sonicated in 2 mL of the methanol−water (7:3, v/v) system for 30 min and then centrifuged at 5000 rpm for 5 min, and the supernatant was filtered through a 0.22 μm membrane. The resulting solution was diluted with a Tris-HCl buffer solution for OTA detection. In addition, three spiked samples with different concentrations (low, medium, and high) of OTA standard solutions were prepared for recovery tests.

3. RESULTS

3.1. Detection Principle of the Dual-Signal Enhanced Fluorescent Aptasensor. Here, a FAM-cDNA-aptamer-SG/GO nanosheet fluorescent aptasensor was constructed for ultrasensitive detection of OTA based on FAM and SG dual-signal enhancement and a competitive mode between aptamer-cDNA and target OTA (Scheme 1). SG was inserted into the groove of the aptamer-cDNA double-stranded structure, while the formed FAM-cDNA-aptamer-SG composite was not

adsorbed onto the GO nanosheet, exhibiting strong fluorescence responses (F_1). Due to the competitive binding of the aptamer and target OTA, the FAM-cDNA-aptamer-SG composite structure was destroyed, resulting in the release of FAM-cDNA and SG, as well as the fluorescence quenching of SG and FAM by the GO nanosheet through FRET (F_2). The OTA-induced change ($\Delta F = F_1 − F_2$) in fluorescence intensity was obtained for quantitation of OTA in standard and sample solutions. The competitive principle between cDNA and OTA to aptamer would significantly enhance the selectivity, and the dual-signal amplification strategy could remarkably improve the detection sensitivity of the developed fluorescent aptasensor for OTA detection in complex matrices.

3.2. Characterization of the Dual-Signal Enhanced Fluorescent Aptasensor. After the fluorescent aptasensor was constructed, it was characterized for subsequent application. First, the fluorescence emission spectrum of FAM and SG fluorophores and the UV−visible absorption spectrum of GO were measured. As shown in Figure 1A, SG
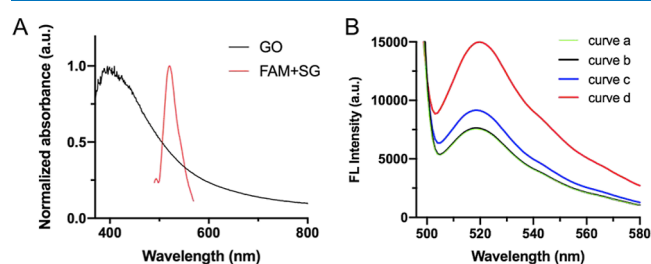
Figure 1. (A) Emission spectrum of FAM and SG and UV−vis absorption spectrum of GO nanosheets. (B) Fluorescence spectra of (a) cDNA-FAM; (b) cDNA-FAM and SG; (c) cDNA-FAM and aptamer; and (d) cDNA-FAM, aptamer, and SG.

and FAM emit fluorescence spectra at the same emission wavelength under the same excitation source. The fluorescence emission spectra of SG and FAM overlapped with the UV−visible spectra of the GO nanosheet. These results confirmed the feasibility of the dual-probe signal amplification strategy and the reliability of FRET between FAM + SG and the GO nanosheet.

Then, the fluorescence emission spectra of the above-prepared solutions *a* of FAM-cDNA, *b* of FAM-cDNA + SG, *c* of FAM-cDNA + aptamer, and *d* of FAM-cDNA + aptamer + SG are recorded in Figure 1B to verify the each-step fabrication of the fluorescent aptasensor. It was noticed that the fluorescence emission spectra of cDNA-FAM (solution *a*) overlapped with that of FAM-cDNA + SG (solution *b*), demonstrating the same excitation and emission characteristics of the two fluorophores, as well as no fluorescence enhancement effect of SG to FAM labeled on single-stranded cDNA. With the introduction of the OTA aptamer, the fluorescence intensity of FAM-cDNA + aptamer (solution *c*) exhibited a slight increase, illustrating the first signal enhancement. However, a remarkably enhanced fluorescence intensity was observed when SG was added to form the FAM-cDNA + aptamer + SG probe (solution *d*), presenting the second fluorescence signal amplification. This further demonstrated that SG could be inserted into the double-stranded FAM-cDNA + aptamer structure to achieve the dual-signal enhanced strategy. The fluorescence signal decreased, and the value of fluorescence intensity change (ΔF) was 3518.6 au upon addition of 0.01 ng/mL of OTA. The above results all

illustrated the successful construction of the fluorescent aptasensor for subsequent detection of OTA.

3.3. Optimization of Experimental Conditions. Aiming to realize the optimal analytical performance of the established aptasensor for OTA detection, some vital experimental conditions including the concentration ratio of aptamer to FAM-cDNA, incubation temperature, the incubation time of the dual-signal probes, and the incubation time of GO nanosheets were systematically optimized in the absence (C_{OTA} = 0 ng/mL) and presence (C_{OTA} = 100 ng/mL) of target OTA.

As SG was inserted into the double-stranded FAM-cDNA-aptamer structure, the added amounts of FAM-cDNA and aptamer should be enough to realize signal amplification and improve the detection sensitivity. Herein, different concentration ratios (0.5:1, 1:1, 1.5:1, and 2:1) of aptamer to FAM-cDNA were considered for the adsorption of SG to measure the fluorescence changes ΔF without (C_{OTA} = 0 ng/mL) and with (C_{OTA} = 100 ng/mL) the introduction of target OTA. Figure 2A illustrates that the largest ΔF value was obtained
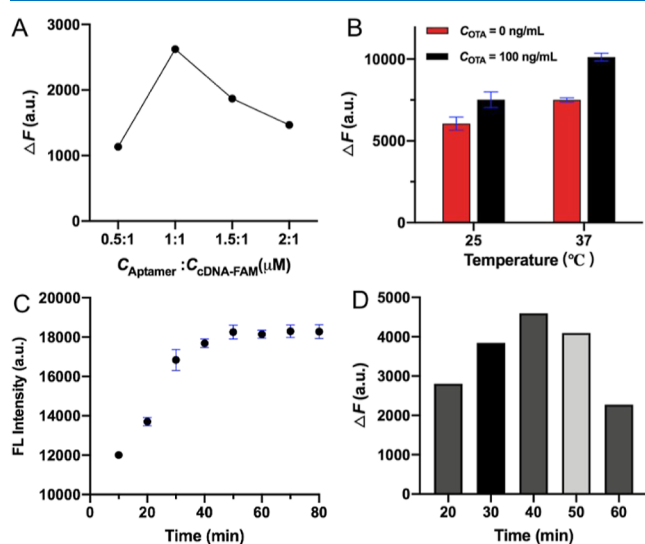
Figure 2. Optimization of experimental conditions: (A) concentration ratio of aptamer and FAM-labeled cDNA; (B) temperature of the reaction; (C) incubation time of the double-stranded structure; and (D) incubation time of GO (n = 3).

when the concentration ratio of aptamer to FAM-cDNA was set to 1:1, which could guarantee the highest adsorption amount of SG and the largest fluorescence quenching efficiency of the GO nanosheet on FAM and SG.

Incubation temperature was an important parameter to provide a stable solution system for subsequent detection. Therefore, two conventional temperature conditions of 25 and 37 °C were taken into account. It can be found in Figure 2B that the larger ΔF values were observed when the incubation system was controlled at 37 °C. This might be since at this temperature, the FAM-cDNA, aptamer, double-stranded FAM-cDNA-aptamer, and SG all maintain their best activities, resulting in the highest binding efficacy of OTA to the aptamer and quenching efficiency of GO nanosheets on the dual-signal fluorescence probes.

Sufficient mixing of SG with the double-stranded FAM-cDNA-aptamer probes would allow the best fluorescence signal enhancement; thus, the incubation time of the dual-signal

probes was optimized at 37 °C. Figure 2C shows that the fluorescence intensity of the FAM-cDNA-aptamer-SG probes gradually increased with increasing incubation time and remained stable after 50 min. Therefore, 50 min was determined as the optimal incubation time for the dual-signal fluorescence probes.

The quenched fluorescence of cDNA-FAM and SG probes by GO nanosheets was directly relevant to the amount of OTA for accurate quantitation. Thus, the incubation time of GO with the OTA-induced released cDNA-FAM and SG probes should be paid more attention. Figure 2D depicts that the ΔF values varied with increasing incubation time, and the biggest ΔF value was obtained when the incubation time was controlled at 40 min.

3.4. Analytical Performance of the Fluorescent Aptasensor for OTA Detection. Under the above-optimized experimental conditions, the developed FAM-cDNA-aptamer-SG/GO nanosheet-based dual-signal enhanced fluorescent aptasensor was adopted for OTA detection at an excitation wavelength of 495 nm and an emission wavelength of 520 nm. With increasing added concentration of OTA into the dual-probe system, the released amounts of FAM-cDNA and SG were increased, accompanied by the increase in the quenched fluorescence intensity and ΔF value. Thus, a significant positive correlation between ΔF and the concentration of OTA (C_{OTA}) is observed in Figure 3. The regression equation was listed as
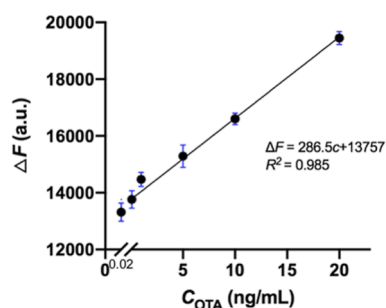
Figure 3. Relationship between the changed fluorescence intensity (ΔF) and the added OTA concentration (0.02−20 ng/mL) (n = 3).

ΔF = 286.5 C_{OTA} + 13,757 (R^2 = 0.985) in a wide linear concentration range of 0.02−20 ng/mL. The limit of detection, which was determined through the infinite dilution of the OTA standard solution, was 0.005 ng/mL. Compared with other sensing methods for OTA detection in Table 1, it could be concluded that the developed dual-signal enhanced fluorescent aptasensor in this study exhibited obvious merits regarding wider linear range and better detection limit than the previously reported sensors. This was beneficial from the remarkably enhanced fluorescence signals of FAM and SG probes, as well as the sensitive FRET effects between FAM, SG, and GO nanosheets.

Then, the accuracy or robustness of the proposed fluorescent aptasensor was evaluated through recovery tests in malt samples for OTA detection. Blank (OTA-free) malt samples were fortified with low (0.5 ng/mL), medium (5 ng/mL), and high (20 ng/mL) concentrations of OTA using the standard addition method, and the sample solutions were then prepared as the above-described procedure for OTA quantitation using the developed dual-signal enhanced fluorescent aptasensor. As shown in Table 2, the average

Table 1. Comparison of the Developed Dual-Signal Enhanced Fluorescent Aptasensor with Other Biosensors for OTA Detection

material	method	linear range (ng/mL)	LOD (ng/mL)	refs
chitosan/hydrogel	electrochemical sensor	0.1–100	0.03	20
Au/Cys/Anti-OTA[a]	electrochemical immunosensor	0.5–100	0.15	21
ZnCdSe QDs/SA-ZnTPyP[b]	fluorescent sensor	0.5–80	0.33	22
CuS-Ab NPs[c]	fluorescent sensor	0.1–100	0.01	23
AP@MBs[d]	fluorescent aptasensor	1–1000	0.63	24
NiO NPs[e]	fluorescent aptasensor	0.5–200	0.49	25
MNPs-Apt[f]	fluorescent aptasensor	0.5–128	0.125	26
FAM-cDNA-Apt-SG-GO	fluorescent aptasensor	0.02–20	0.005	This work

[a]Gold/cysteamine/anti-OTA antibody. [b]ZnCdSe quantum dots and assembled zinc porphyrin. [c]Antibody-conjugated copper monosulfide nanoparticles. [d]OTA aptamer-functionalized magnetic beads. [e]Nickel oxide nanoparticles. [f]Aptamer-coupled magnetic nanomaterials.

recoveries ranged from 91.37 to 116.83%, which were acceptable and satisfactory.

Table 2. Recovery Measured by the Proposed Fluorescent Aptasensor in the Fortified Malt Samples ($n = 3$)

sample	added amount (ng/mL)	measured amount (ng/mL)	recovery (%)
1#	0.5	0.58 ± 0.12	116.83
2#	5	4.57 ± 0.78	91.37
3#	20	18.29 ± 2.53	91.44

These results suggested the good feasibility and reliability of the newly developed dual-signal fluorescent aptasensor for OTA detection in real samples.

3.5. Specificity Analysis. To examine the selectivity and anti-interference ability of the developed fluorescent aptasensor for specific detection of OTA, four mycotoxins of DON, ZEN, AFB$_1$, and T-2 toxin at 100 ng/mL that were commonly found in foods and other matrices were selected as the interferents. As presented in Figure 4, 20 ng/mL of OTA
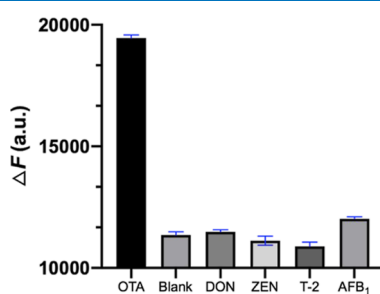
Figure 4. Specificity of the fluorescence aptasensor assay toward OTA against other mycotoxins and blank sample ($n = 3$).

caused extremely higher ΔF values (around 19,000 au) than 100 ng/mL of four tested mycotoxins, illustrating that only OTA could induce a significant change in the fluorescence responses of the dual-signal probes and other interfering substances would not affect OTA detection. These also confirmed the superior selectivity and specificity of the developed fluorescent aptasensor for target OTA.

3.6. Real Sample Analysis. To further verify the practicability of the proposed fluorescent aptasensor, ten batches of real malt matrices including five normal (S1−S5) and five moldy (S6−S10) samples were tested for contamination levels of OTA. As shown in Table 3, the five normal malt samples purchased from pharmacies in Beijing, China,

Table 3. Detection of OTA in Normal and Moldy Malt Samples

sample	no.	measured amount (μg/kg)
normal malt sample	S1	
	S2	
	S3	
	S4	
	S5	
moldy malt sample	S6	5.40
	S7	1.20
	S8	
	S9	7.72
	S10	

and sealed in the packages were not detected with OTA. However, after the five normal samples were placed in an environment with high humidity and constant temperature for some time, obvious mold floras were observed, and OTA was measured in three (3/5) samples with contamination levels of 1.20−7.72 μg/kg. Notably, OTA contents in two samples exceeded the permitted MRL (5.0 μg/kg). These findings demonstrated that the malt matrix was prone to be contaminated by OTA and that the newly developed dual-signal enhanced fluorescent aptasensor could be potentially applied to sensitively monitor OTA residual levels in actual malt samples.

4. DISCUSSION

In conclusion, a FAM-cDNA-aptamer-SG/GO nanosheet-based dual-signal enhanced fluorescent aptasensor via FRET between FAM and SG as the donor and GO nanosheet as the acceptor was developed for simple, sensitive, low-cost, and rapid detection of trace OTA in complex matrices. FAM and SG with strong fluorescence responses were regarded as the fluorophores, and the FAM-cDNA-aptamer double-stranded structure was helpful for the adsorption of abundant SG probes to remarkably enhance the fluorescence signals for highly sensitive detection of OTA. Under the optimized conditions, low to 0.005 ng/mL of OTA could be detected by the developed fluorescent aptasensing platform in a wide concentration range of 0.02−20 ng/mL. The constructed fluorescence sensor exhibited slight variations in parallel detection outcomes and high precision and did not necessitate a laborious pretreatment procedure, thereby significantly reducing time and expenses. In addition, the aptasensor allowed high selectivity for OTA over other interfering substances as well as superior reliability and practicability in

actual malt samples. By altering the corresponding aptamer, the proposed fluorescent aptasensing platform could be extended to more contaminants or trace molecules in food, environmental, and diagnostic fields.

■ AUTHOR INFORMATION

Corresponding Author

Weijun Kong − *School of Traditional Chinese Medicine, Capital Medical University, Beijing 100069, China; Laboratory for Clinical Medicine, Capital Medical University, Beijing 100069, China;* ⊙ orcid.org/0000-0001-9943-7218; Email: kongwj302@126.com

Authors

Xueying Li − *School of Traditional Chinese Medicine, Capital Medical University, Beijing 100069, China*

Te Li − *School of Traditional Chinese Medicine, Capital Medical University, Beijing 100069, China*

Jiahuai Zhang − *Center for Clinical Laboratory, Capital Medical University, Beijing 100069, China*

Qing Zhang − *Key Laboratory of Modern Preparation of TCM, Ministry of Education, Pharmacy College, Jiangxi University of Traditional Chinese Medicine, Nanchang 330004, China*

Kai Deng − *School of Traditional Chinese Medicine, Capital Medical University, Beijing 100069, China*

Runran Ma − *School of Traditional Chinese Medicine, Capital Medical University, Beijing 100069, China*

Jiabo Wang − *School of Traditional Chinese Medicine, Capital Medical University, Beijing 100069, China*

Complete contact information is available at:
https://pubs.acs.org/10.1021/acsomega.4c00377

Author Contributions

X.L., Q.Z., and W.K. conceived the idea, designed the experiments, and analyzed the results; J.Z. and K.D. contributed reagents; X.L., T.L., and Q.Z. carried out the experiments; R.M. and J.W. carried out visualization of the data; X.L. and Q.Z. wrote and edited the manuscript. J.W. and W.K. reviewed the manuscript. All the authors approved the final manuscript.

Notes

The authors declare no competing financial interest.

■ REFERENCES

(1) Hou, Y. J.; Jia, B. Y.; Sheng, P.; Liao, X. F.; Shi, L. C.; Fang, L.; Zhou, L. D.; Kong, W. J. Aptasensors for mycotoxins in foods: Recent advances and future trends. *Compr. Rev. Food Sci. Food Saf.* **2022**, *21*, 2032−2073.

(2) Chen, J. S. Essential role of medicine and food homology in health and wellness. *Chin. Herb. Med.* **2023**, *15*, 347−348.

(3) Liao, X. F.; Li, Y.; Long, N.; Xu, Q. B.; Li, P.; Wang, J. B.; Zhou, L. D.; Kong, W. J. Multi-mycotoxin detection and human exposure risk assessment in medicinal foods. *Food Res. Int.* **2023**, *164*, 112456.

(4) Schrenk, D.; Bodin, L.; Chipman, J. K.; del Mazo, J.; Grasl-Kraupp, B.; Hogstrand, C.; Hoogenboom, L. R.; Leblanc, J.; Nebbia, C. S.; et al. Risk assessment of ochratoxin A in food. *EFSA J.* **2020**, *18*, 6113.

(5) Obafemi, B. A.; Adedara, I. A.; Rocha, J. B. T. Neurotoxicity of ochratoxin A: Molecular mechanisms and neurotherapeutic strategies. *Toxicology* **2023**, *497−498*, 153630.

(6) Hou, Y. J.; Long, N.; Jia, B. Y.; Liao, X. F.; Yang, M. H.; Fu, L. Z.; Zhou, L. D.; Sheng, P.; Kong, W. J. Development of a label-free electrochemical aptasensor for ultrasensitive detection of ochratoxin A. *Food Control* **2022**, *135*, 108833.

(7) Cheng, J. X.; Liang, L. W.; Liu, Y. J.; Yang, M.; Liu, X. X.; Hou, Y. Y.; Shui, J. Y.; Li, D. Y.; Wu, Q.; Liu, H.; et al. Expression, purification of codon-optimized ochratoxin A nanobody-GST fusion protein and its one-step immunoassay for detection of OTA in cereal. *J. Food Compos. Anal.* **2023**, *123*, 105530.

(8) Keskin, E.; Eyupoglu, O. E. Determination of mycotoxins by HPLC, LC-MS/MS and health risk assessment of the mycotoxins in bee products of Turkey. *Food Chem.* **2023**, *400*, 134086.

(9) Zhang, J.; Lu, Y. H.; Gao, W.; Yang, P.; Cheng, N. S.; Jin, Y. W.; Chen, J. B. Structure-switching locked hairpin triggered rolling circle amplification for ochratoxin A (OTA) detection by ICP-MS. *Microchem. J.* **2023**, *186*, 108365.

(10) Li, P.; Luo, C.; Chen, X. X.; Huang, C. B. A novel "off-on" ratiometric fluorescent aptasensor for adenosine detection based on FRET between quantum dots and graphene oxide. *Spectrochim. Acta, Part A* **2024**, *305*, 123557.

(11) Liu, L.; Hong, J. C.; Wang, W. H.; Xiao, S.; Xie, H. Z.; Wang, Q. Q.; Gan, N. Fluorescent aptasensor for detection of live foodborne pathogens based on multicolor perovskite-quantum-dot-encoded DNA probes and dual-stirring-bar-assisted signal amplification. *J. Pharm. Anal.* **2022**, *12*, 913−922.

(12) Yang, Y. K.; Zeng, X. X.; Tian, Y.; Wang, X. M.; Jing, X.; Yu, L. G.; Bai, B. Q.; Zhang, J. H.; Qin, S. A universal design of turn-on fluorescent aptasensor based on luminescent MOFs: Application for the detection of bisphenol A in water, milk and chicken samples. *Food Chem.* **2023**, *422*, 136167.

(13) Zhao, L. P.; Li, L. S.; Zhao, Y.; Zhu, C.; Yang, R. Q.; Fang, M. Q.; Luan, Y. X. Aptamer-based point-of-care-testing for small molecule targets: From aptamers to aptasensors, devices and applications. *TrAC, Trends Anal. Chem.* **2023**, *169*, 117408.

(14) Setlem, S. K.; Mondal, B.; Ramlal, S. A fluorescent aptasensor for the detection of Aflatoxin B$_1$ by graphene oxide mediated quenching and release of fluorescence. *J. Microbiol. Methods* **2022**, *193*, 106414.

(15) Nemati, F.; Hosseini, M. Fluorescence turn-on detection of miRNA-155 based on hybrid Ce-MOF/PtNPs/graphene oxide serving as fluorescence quencher. *J. Photochem. Photobiol., A* **2022**, *429*, 113943.

(16) Li, Q. X.; Kang, Y.; Yin, S. X.; Qian, Y.; Cai, Y. F.; Yang, Z. Q. Graphene oxide synergy with the conjugation of DNA and quantum dots for the sensitive detection of ochratoxin A. *Food Anal. Methods* **2022**, *15*, 440−447.

(17) Li, S.; Kang, Y.; Shang, M. D.; Cai, Y. F.; Yang, Z. Q. Highly sensitive and selective detection of ochratoxin A using modified graphene oxide-aptamer sensors as well as application. *Microchem. J.* **2022**, *179*, 107449.

(18) Chen, S.; Liu, Y. J.; Zhai, F.; Jia, M. Novel label-free fluorescence aptasensor for chloramphenicol detection based on a DNA four-arm junction-assisted signal amplification strategy. *Food Chem.* **2022**, *366*, 130648.

(19) Guo, Z. J.; Tian, J.; Cui, C. B.; Wang, Y.; Yang, H. H.; Yuan, M.; Yu, H. S. A label-free aptasensor for turn-on fluorescent detection of ochratoxin A based on SYBR Gold and single walled carbon nanohorns. *Food Control* **2021**, *123*, 107741.

(20) Li, X. Y.; Falcone, N.; Hossain, M. N.; Kraatz, H. B.; Chen, X. J.; Huang, H. Development of a novel label-free impedimetric electrochemical sensor based on hydrogel/chitosan for the detection of ochratoxin A. *Talanta* **2021**, *226*, 122183.

(21) de Oliveira, J. P.; Burgos-Flórez, F.; Sampaio, I.; Villalba, P. V.; Zucolotto, V. Label-free electrochemical immunosensor for Ochratox-in a detection in coffee samples. *Talanta* **2023**, *260*, 124586.

(22) Liu, L.; Huang, Q. W.; Tanveer, Z. I.; Jiang, K. Q.; Zhang, J. H.; Pan, H. Y.; Luan, L. J.; Liu, X. S.; Han, Z.; Wu, Y. J. "Turn off-on" fluorescent sensor based on quantum dots and self-assembled porphyrin for rapid detection of ochratoxin A. *Sens. Actuators, B* **2020**, *302*, 127212.

(23) Chen, R. P.; Sun, Y. F.; Huo, B. Y.; Zhao, X. D.; Huang, H.; Li, S.; Bai, J. L.; Liang, J.; Gao, Z. X. A copper monosulfide-nanoparticle-based fluorescent probe for the sensitive and specific detection of ochratoxin A. *Talanta* **2021**, *222*, 121678.

(24) Han, B.; Fang, C.; Sha, L. J.; Jalalah, M.; Al-Assiri, M. S.; Harraz, F. A.; Cao, Y. Cascade strand displacement reaction-assisted aptamer-based highly sensitive detection of ochratoxin A. *Food Chem.* **2021**, *338*, 127827.

(25) Khan, A.; Azhar Hayat Nawaz, M.; Akhtar, N.; Raza, R.; Yu, C.; Andreescu, S.; Hayat, A. Morphology controlled NiO nanostructures as fluorescent quenchers for highly sensitive aptamer-based FRET detection of ochratoxin A. *Appl. Surf. Sci.* **2021**, *566*, 150647.

(26) Wu, R. Y.; Guo, J. P.; Wang, M. K.; Liu, H. M.; Ding, L. H.; Yang, R. Y.; Liu, L. E.; Liu, Z. Y. Fluorescent sensor based on magnetic separation and strand displacement amplification for the sensitive detection of ochratoxin A. *ACS Omega* **2023**, *8*, 15741−15750.